

OCCLE: LABEL-EFFICIENT 3D SEMANTIC OCCUPANCY PREDICTION

Naiyu Fang¹, Zheyuan Zhou², Fayao Liu³, Xulei Yang³, Jiacheng Wei⁴, Lemiao Qiu², Guosheng Lin^{1,4*}

¹S-Lab, Nanyang Technological University, Singapore

²School of Mechanical Engineering, Zhejiang University, China

³Institute for Infocomm Research, A*STAR, Singapore

⁴School of Computer Science and Engineering, Nanyang Technological University, Singapore

{naiyu.fang, jiacheng.wei, gslin}@ntu.edu.sg

{zheyuanzhou, qiulm}@zju.edu.cn

{fayaoliu, yangxulei}@gmail.com

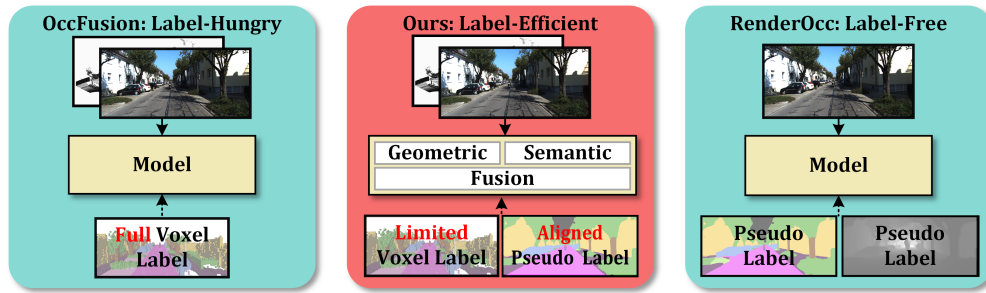


Figure 1: Label-efficient 3D semantic occupancy prediction aims to achieve high performance using limited voxel annotations and aligned pseudo label. We propose OccLE, a novel learning paradigm that decouples semantic and geometric learning and fuse their feature grids for the final prediction.

ABSTRACT

3D semantic occupancy prediction offers an intuitive and efficient scene understanding and has attracted significant interest in autonomous driving perception. Existing approaches either rely on full supervision, which demands costly voxel-level annotations, or on self-supervision, which provides limited guidance and yields suboptimal performance. To address these challenges, we propose **OCCLE**, a **Label-Efficient 3D Semantic Occupancy Prediction** that takes images and LiDAR as inputs and maintains high performance with limited voxel annotations. Our intuition is to decouple the semantic and geometric learning tasks and then fuse the learned feature grids from both tasks for the final semantic occupancy prediction. Therefore, the semantic branch distills 2D foundation model to provide aligned pseudo labels for 2D and 3D semantic learning. The geometric branch integrates image and LiDAR inputs in cross-plane synergy based on their inherency, employing semi-supervision to enhance geometry learning. We fuse semantic-geometric feature grids through Dual Mamba and incorporate a scatter-accumulated projection to supervise unannotated prediction with aligned pseudo labels. Experiments show that OccLE achieves competitive performance with only 10% of voxel annotations, reaching a mIoU of 16.59% on the SemanticKITTI validation set.

Keywords Autonomous Driving · 3D Semantic Occupancy Prediction · Label-Efficient Learning

*Corresponding author. Guosheng Lin (e-mail: gslin@ntu.edu.sg)

1 Introduction

3D perception task is foundational cornerstone for autonomous driving systems. Among various perception methods, 3D semantic occupancy prediction [1, 2, 3] has garnered significant attention for providing intuitive and efficient scene understanding for downstream tasks. This task aims to estimate the occupancy status and semantic label of each voxel in a 3D grid, given input from 2D images, 3D LiDAR, or a combination of both.

Previous studies [4, 5] proposed numerous supervised learning paradigms with diverse modal inputs. A notable challenge is that their high performance relies heavily on extensive voxel annotations, which are both costly and labor-intensive. The cubic complexity of the voxel grid leads to a substantial workload during manual annotation. Even with pre-annotated 3D labels generated using auto-labeling assistants, one hour of human labor just only annotates 10 frames [6, 7]. This issue limits the scalability of supervised methods for real-world deployment, especially in terms of robustness.

Recent advancements in 3D semantic occupancy prediction have shifted towards a label-free paradigm. These self-supervised methods leverage existing vision foundation models to generate various pseudo labels for auxiliary supervision, such as image semantic segmentation [8], depth information [9], and LiDAR segmentation [10]. To bridge the 3D representation with 2D pseudo label, specific 3D representation formats have been proposed to facilitate volume rendering, including signed distance functions[7] and 3D Gaussians [11]. The core strategy of these self-supervised methods is to supplement pseudo semantic supervision. They project LiDAR segmentation annotations from the same dataset into 2D pseudo labels [12, 6]. However, this pseudo labels generation still is expensive and provides only sparse supervision. They also employ a 2D vision foundation model to generate 2D pseudo labels [7], which suffers from class misalignment. For the overall pipeline, they supervise only the final prediction using 2D pseudo labels and do not apply separate supervision to geometric and semantic feature learning. Thus, this non-decoupled design leads to insufficient geometric learning, which reduces volume-rendering quality and weakens semantic supervision.

To address these challenges, we propose OccLE, a label-efficient 3D semantic occupancy prediction method, as illustrated in Fig. 1, which uses limited voxel annotations while maintaining high performance. We design the label-efficient learning paradigm: taking image and LiDAR scan inputs, fully decoupling semantic and geometric feature learning, fusing their feature grids for 3D semantic occupancy prediction, and supervising with limited voxel annotations and aligned pseudo labels. Specifically, OccLE consists of the semantic branch, the geometric branch, and semantic-geometric feature grid fusion. The semantic branch distills dataset-specific and open-vocabulary 2D foundation models to produce aligned pseudo labels for supervising 2D and 3D semantic learning, independently of geometry. The geometric branch integrates image and LiDAR and inputs in cross-plane synergy based on their inherent characteristics, employing semi-supervision to enhance geometry learning. The semantic-geometric feature grid fusion employs Dual Mamba to fuse the two feature grids for lightweight long-range relationship modeling, and introduces a scatter-accumulated projection to guide unannotated predictions with aligned pseudo labels, without relying on any specific feature grid format. In summary, the main contributions of this work are summarized as follows: In summary, the main contributions of this work are summarized as follows:

- We introduce a label-efficient 3D semantic occupancy prediction task and a learning paradigm that decouples semantic and geometric learning, followed by their synergistic integration. The model is supervised using limited voxel annotations and aligned pseudo labels to achieve high performance.
- We present three techniques: distilling 2D foundation model for 2D and 3D semantic learning; semi-supervised geometry learning using cross-plane image and LiDAR feature synergy; and semantic-geometric feature grids fusion with auxiliary supervision by scatter-accumulated projection.
- Experimental results show that OccLE achieves competitive performance compared to fully supervised methods, attaining 16.59 % mIoU on the SemanticKITTI validation set using only 10 % of the voxel annotations.

2 Related Works

2.1 3D Semantic Occupancy Prediction

3D semantic occupancy prediction, also referred to as the semantic scene completion (SSC), was first introduced by SSCNet [1]. In SSCNet, image features are lifted into a 3D representation to predict voxel-level semantics. With the advancement of autonomous driving [2, 3], SSC has attracted significant attention for providing clear and efficient scene representations. Based on the type of input, SSC methods can be categorized into camera-based and multi-modal methods.

For camera-based 3D semantic occupancy prediction, a key challenge lies in lifting 2D to 3D representations. Previous works [13, 14, 15] utilize calibration and depth information to establish explicit backwards projections. ViewFormer [16] proposes a learning-first attention mechanism to aggregate multi-view features. Some studies [17, 18] represent scenes using sparse 3D semantic Gaussians. TPVFormer [19] introduces three perpendicular views (TPV) to enhance the interaction of image features.

Since dimensional transformation based on depth estimation is ill-posed for camera-based methods, multi-modal method incorporates LiDAR and radar inputs to obtain accurate distance measurements. Its essential research is modal fusion. OccFusion [5] directly concatenates feature channels. MetaOcc [20] learn global and local alignment to enhance fused representations. Some studies [21, 22] advance fusion by employing point-to-point queries from 3D to 2D. OccGen [23] employs a diffusion model to refine the fused features.

Building on prior work, OccLE takes camera images and a LiDAR scans as inputs, applies backward projection to derive 3D feature grids from 2D image feature maps, and proposes a lightweight yet effective fusion strategy in the geometry learning termed cross-plane image and LiDAR feature synergy.

2.2 Label-efficient learning

Label-efficient learning seeks to minimize the reliance on large amounts of label while maintaining high model performance. Prior works have proposed novel learning paradigms to achieve this, such as semi-supervised learning and self-supervised learning. Semi-supervised learning [24] combines a small labeled dataset with abundant unlabeled data to improve model generalization, while self-supervised learning [25] generates supervision directly from unlabeled data through pretext tasks.

In label-efficient learning for 3D semantic occupancy prediction, self-supervision methods render 3D feature into 2D representations, and supervise with labels from other tasks. To facilitate rendering, SelfOcc [7] introduces a signed distance function-based representation, while GaussTR [11] proposes a 3D Gaussian-based representation. For auxiliary supervision, OccFlowNet [12] utilizes projected semantic point clouds, whereas RenderOcc [6] relies on depth estimation and image segmentation.

Inspired by the above, OccLE utilizes the pseudo label from image segmentation as a key supervision to enable label-efficient learning. We distill 2D foundation model for multi-modal semantic learning, while supervising the accumulated projection in the final prediction.

3 Methodology

3.1 Overview

We aim to take multi-frame camera images $\{\mathbf{I}_{t-i}\}_{i=0}^{N-1} \in \mathbb{R}^{h \times w}$, multi-frame point clouds $\{\mathbf{P}_{t-i}\}_{i=0}^{N-1} \in \mathbb{R}^{n \times 4}$, camera calibration $\{\mathbf{K}, \mathbf{T}\}$ as inputs to predict the 3D semantic occupancy $\mathbf{Y}_t \in \{c_0, c_1, \dots, c_{M-1}\}^{H \times W \times Z}$ at timestep t . To enable label-efficient training, we supervise the model using only limited voxel annotations (e.g., 10% $\{\bar{\mathbf{Y}}_t\}$ of all samples). Here, \mathbf{K}, \mathbf{T} represent the intrinsic and extrinsic camera matrices, respectively; $\{\bar{\mathbf{Y}}_t\}$ is the ground truth of 3D semantic occupancy prediction. N denotes frame number; M denotes class number, h and w denote the height and width of camera image; H, W , and Z represent the length, width, height of voxel grid. Our method is formulated as $\mathbf{Y}_t = \Theta \left(\{\mathbf{I}_{t-i}\}_{i=0}^{N-1}, \{\mathbf{P}_{t-i}\}_{i=0}^{N-1}, \mathbf{K}, \mathbf{T} \right)$, where Θ is our proposed OccLE. For clarity, we omit the timestep subscript t for all variables in the following description.

The overview of OccLE is illustrated in Fig. 2. For simplicity, only a single input frame is shown. To enable label-efficient learning, our pipeline comprises three components: a semantic branch, a geometric branch, and a semantic-geometric feature grid fusion module. We decouple the semantic and geometric learning with distinct supervision strategies, and fuse their feature grids to predict 3D semantic occupancy. In the semantic branch, we distill 2D foundation models to predict aligned pseudo labels and supervise 2D and 3D semantic feature learning. In the geometric branch, we synergize image and LiDAR features based on their inherency and employ semi-supervision to strengthen geometry learning. In the semantic-geometric feature grid fusion module, we employ Dual Mamba to fuse feature grids and employ scatter-accumulated projection to supervise unannotated predictions with aligned pseudo labels. The semantic branch, the geometric branch, and the semantic-geometric feature grid fusion will be discussed in Sec. 3.2, Sec. 3.3, and Sec. 3.4, respectively.

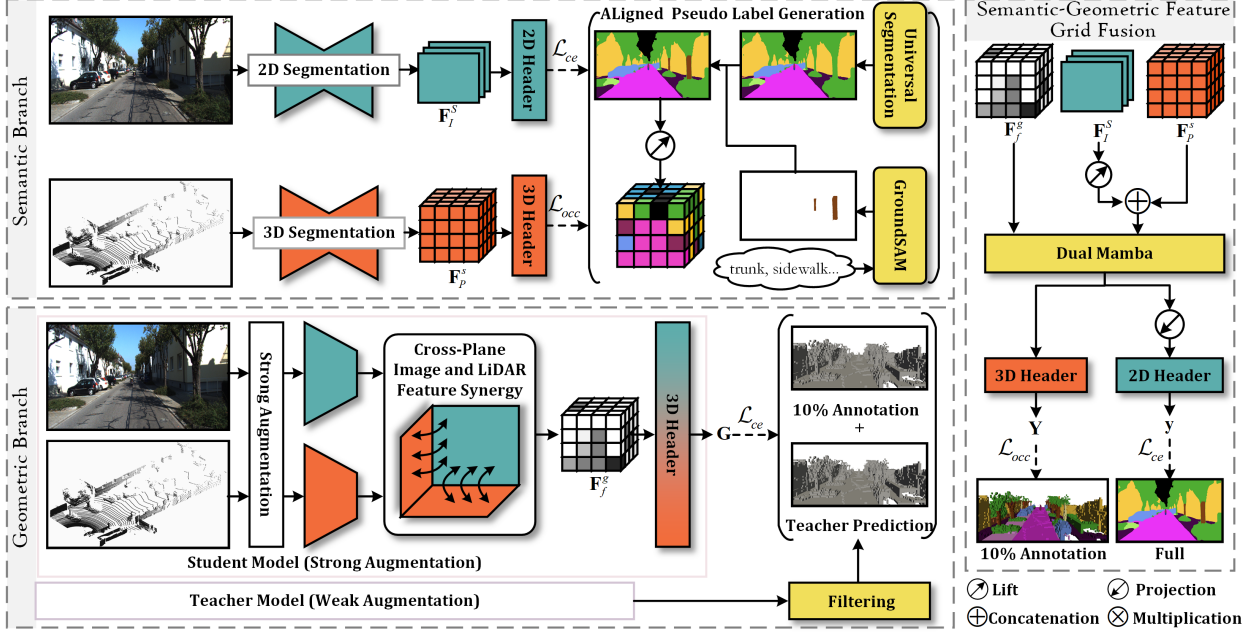


Figure 2: The overview of OccLE. First, we distill 2D foundation models to predict aligned pseudo labels for supervising 2D and 3D semantic learning. Next, we propose cross-plane image and LiDAR feature synergy and apply semi-supervision to learn geometry. Finally, we fuse semantic and geometric feature grids via Dual Mamba and supervise the unannotated prediction with aligned pseudo label using scatter-accumulated projection.

3.2 Distill 2D Foundation Models for 2D and 3D Semantic Learning

3D semantic occupancy prediction is implemented through the entanglement of geometric and semantic features [4]. The geometric feature indicates whether a voxel is occupied, while the semantic feature specifies the class occupying the voxel. 3D semantic occupancy prediction maps the feature grid to voxel semantic labels. Achieving high accuracy traditionally requires extensive voxel annotations to guide the mapping, but obtaining such annotations is costly. To mitigate this requirement, we notice that the image semantic segmentation maps the feature map to pixel semantic label and benefits from large annotated datasets. Therefore, we aim to distill 2D foundation model for 2D and 3D semantic learning, where the 2D foundation model predicts aligned pseudo labels to supervise the semantic learning of image and LiDAR scan inputs.

2D foundation models may not share the same class definitions as 3D semantic occupancy prediction. For example, a 2D foundation model trained on the Cityscapes dataset [26] does not include categories such as bicyclist or truck when applied to the SemanticKITTI dataset [27]. To resolve this class misalignment, we integrate both dataset-specific and open-vocabulary 2D foundation models. The dataset-specific one produces primary labels for shared classes, while the open-vocabulary one produces auxiliary labels for unaligned classes. Specifically, we utilize MSeg [28] as a dataset-specific model and SAM2 [8] for open-vocabulary model. We adapt MSeg universal class classification to the task-specific classes, input the unaligned class name prompts into SAM2, and merge outputs using Boolean operations to generate aligned pseudo labels \bar{s} .

We employ \bar{s} to fully supervise semantic learning of images and LiDAR scans, enabling lightweight deployment via distillation. Specifically, we employ a UNet [29] \mathcal{G}_{s2d} to extract features map \mathbf{F}_I^s from the image \mathbf{I} . We adopt the voxelization in VoxelNet [30] and utilize a sparse UNet3D [31] \mathcal{G}_{s3d} to extract features grid \mathbf{F}_P^s from the LiDAR scan \mathbf{P} . The mathematical expression is given by:

$$\begin{cases} \mathbf{F}_I^s = \mathcal{G}_{s2d}(\mathbf{I}) \\ \mathbf{F}_P^s = \mathcal{G}_{s3d}(\mathcal{V}(\mathbf{P})) \end{cases} \quad (1)$$

where \mathcal{V} refers to the voxelization process, which randomly samples up to 35 points per voxel. Each point includes its position, intensity, and the offset from the voxel center.

The semantic branch predicts image segmentation $\bar{\mathbf{s}}$ and LiDAR segmentation $\bar{\mathbf{S}}$ using a 2D header and 3D header. To supervise $\bar{\mathbf{S}}$, we lift $\bar{\mathbf{s}}$ to $\bar{\mathbf{S}}$ as follows:

$$\bar{\mathbf{S}} = \mathcal{F}(\bar{\mathbf{s}}, \mathbf{p}), \mathbf{p} = \mathbf{K}(\mathbf{T} \cdot \mathbf{P}) \quad (2)$$

where \mathcal{F} denotes the sampling function, \mathbf{P} denote the voxel grid coordinates, \mathbf{p} represent the corresponding projected coordinates on the image plane.

3.3 Semi-Supervised Geometry Learning

Prior works [4, 32] depend on absolute depth in learning geometry for 3D semantic occupancy prediction. Because depth estimation is ill-posed, reducing voxel annotations exacerbates uncertainty in this sequential prediction. Since depth is sourced from the LiDAR scan projected on the image plane, we directly use image and LiDAR scan inputs, propose a lightweight and modality-complementary geometry learning module, termed cross-plane image and LiDAR feature synergy, and employ a semi-supervision to learn an accurate geometric feature grid with limited voxel annotations.

3.3.1 Cross-Plane Image and LiDAR Feature Synergy

First, we examine the characteristics of the image and LiDAR scan inputs. As shown by the red boxes in Fig. 3a and Fig. 3b, the frontal-view LiDAR scan is sparse and omits information in the upper region, whereas the image offers continuous context. In the bird’s-eye view (BEV), the image cannot resolve distances along each ray, while the LiDAR scan provides accurate range measurements. In summary, the image is reliable on the yz -plane and the LiDAR scan is reliable along the x -axis in world coordinates. Motivated by their inherency and inspired by [33], we project each their feature grid into its optimal plane in the TPV and fuse them via multiplicative integration.

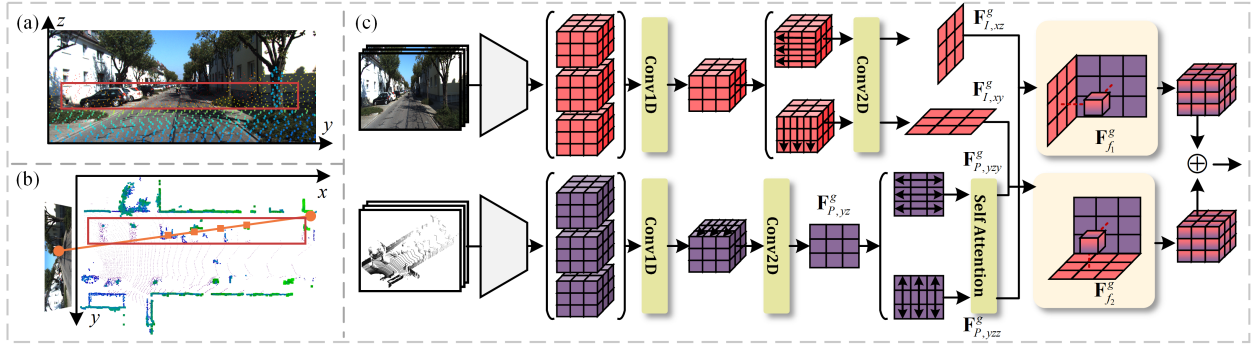


Figure 3: Illustration of geometry learning. (a) Frontal view feature comparison. (b) BEV view feature comparison. (c) The cross-plane image and LiDAR feature synergy.

The cross-plane image and LiDAR feature synergy is illustrated in Fig. 3c. We voxelize multi-frame LiDAR scans using the VoxelNet [30] and process them with a sparse 3D encoder to obtain LiDAR feature grids. In parallel, we extract feature maps from multi-frame images using a 2D encoder and lift into the feature grid defined in Equ. 2. We fuse the multi-frame feature grids into a single grid via a Conv1D layer. For the LiDAR feature grid, we stack along the y and z axes and apply a Conv2D layer to produce feature maps $\mathbf{F}_{I,xz}^g \in \mathbb{R}^{H_1 \times Z_1}$ and $\mathbf{F}_{I,xy}^g \in \mathbb{R}^{W_1 \times Z_1}$. For the image feature grid, we stack along the x -axis and apply a Conv2D layer to generate feature map $\mathbf{F}_{P,yz}^g \in \mathbb{R}^{H_1 \times W_1}$. To enhance $\mathbf{F}_{P,xy}^g \in \mathbb{R}^{H_1 \times W_1}$, we apply self-attention (SA) along the y and z axes, yielding feature maps $\mathbf{F}_{P,yzy}^g \in \mathbb{R}^{H_1 \times W_1}$, $\mathbf{F}_{P,yzz}^g \in \mathbb{R}^{H_1 \times W_1}$ as follows:

$$\begin{cases} \mathbf{F}_{P,yzy}^g = \mathbf{F}_{P,yz}^g + SA\left(\mathbf{F}_{P,yz}^g\right) \\ \mathbf{F}_{P,yzz}^g = \mathbf{F}_{P,yz}^g + SA\left(\mathbf{F}_{P,yz}^{gT}\right)^T \end{cases} \quad (3)$$

We fuse the image and LiDAR feature maps via matrix multiplication in the TPV. The fused feature grids $\mathbf{F}_{f_1}^g, \mathbf{F}_{f_2}^g \in \mathbb{R}^{H_1 \times W_1 \times Z_1}$ are defined as follows:

$$\begin{cases} \mathbf{F}_{f_1}^g = \mathbf{F}_{I,xz}^g \times \mathbf{F}_{P,yzz}^g \\ \mathbf{F}_{f_2}^g = \mathbf{F}_{I,xy}^g \times \mathbf{F}_{P,yzy}^g \end{cases} \quad (4)$$

We add $\mathbf{F}_{f_1}^g$ and $\mathbf{F}_{f_2}^g$ to generate the geometric feature grid \mathbf{F}_f^g and predict geometry $\mathbf{G} \in \mathbb{R}^{H \times W \times Z}$ via a 3D header.

In the proposed workflow, feature grids are converted into feature maps by stacking and subsequently reconstructed into feature grids during the final fusion. In contrast to the 3D attention mechanisms adopted in [4, 32, 34], the cross-plane image and LiDAR feature synergy employs only Conv1D, Conv2D, and SA (with computational complexity $\mathcal{O}(H_1^2)$ or $\mathcal{O}(W_1^2)$) to learn features, making it more lightweight and suitable for real-time applications.

3.3.2 Semi-Supervised Pipeline

To facilitate cross-plane image and LiDAR feature synergy training with limited voxel annotations, we adopt the weak-to-strong consistency principle [35] within a semi-supervised learning. The teacher and student models share the same structure. Table 1 lists their data-augmentation strategy.

Table 1: Data augmentation strategy. The number of signs indicates the augmentation strength.

	Image					LiDAR scan	
	Brightness	HSV space	Motion blur	Weather sim.	Cutout	Point dropout	Voxelization
Teacher	✓	✓	✗	✗	✗	✓	✓
Student	✓✓✓	✓✓✓	✓✓	✓✓	✓	✓✓✓	✓✓✓

We classify image augmentations by their effects on features. Brightness, contrast, and HSV adjustments modify global characteristics and constitute weak augmentation. Weather simulation and motion blur degrade feature clarity and serve as middle augmentation. Cutout removes entire regions of the feature map and thus represents strong augmentation. For LiDAR scans, we vary augmentation strength by adjusting the dropout probability, the dropout number, and the sampling number.

During knowledge distillation, we filter the predictions of teacher model based on confidence scores, which are computed as the maximum channel prediction for each sample. We then concatenate the filtered predictions with the limited voxel annotations to supervise the student model.

3.4 Semantic-Geometric Feature Grid Fusion

In this section, we fuse semantic and geometric feature grids to predict 3D semantic occupancy. Previous works [32, 34] employs attention mechanisms to enable long-range interactions within the feature grid. However, with sequence length HWZ , 3D DA still incurs substantial computational overhead. Recent work [36] adapts Mamba [17] module for efficient long-range dependency learning in this task. Inspired by this approach and given the spatial alignment of our semantic and geometric feature grids, we propose a Dual Mamba that process semantic and geometric feature grids independently, exchanges subsets of their channels for fusion. Specifically, we lift the feature map \mathbf{F}_I^s to a feature grid via Equ. 2 and combine it with \mathbf{F}_P^s to yield the semantic feature grid \mathbf{F}_f^s , Dual mamba then takes \mathbf{F}_f^s and \mathbf{F}_f^g as input and outputs the fused feature grid \mathbf{F}_{3d}^f . The detailed structure of Dual Mamba is illustrated in Appendix A.

GaussTR [11] projects Gaussian feature grids onto the image plane and supervises predictions using pseudo labels from 2D segmentation. Inspired by this approach and aiming to leverage the aligned pseudo label \bar{s} for supervising 3D semantic occupancy prediction, we propose a simple and effective method, termed scatter-accumulated projection, as follows:

$$\mathbf{F}_{2d}^f = \sum_{\mathbf{p}} \mathbf{F}_{3d}^f \quad (5)$$

where $\sum_{\mathbf{p}}(\cdot)$ denotes scattered accumulation over index \mathbf{p} . This operation projects \mathbf{F}_{3d}^f onto the image plane and aggregates projected feature along each ray. It enables the model to identify the semantic class of each feature grid and to capture occlusion and occupancy states in geometry, thereby facilitating both semantic and geometric supervision. Additionally, this method is agnostic to the specific format of the feature grid, thus offering better scalability.

We use a 3D header and 2D header to predict the 3D semantic occupancy \mathbf{Y} and the projected segmentation $\mathbf{y} \in \mathbb{R}^{h \times w}$ from feature grid \mathbf{F}_{3d}^f and projected feature map \mathbf{F}_{2d}^f .

3.5 Losses and Training Strategy

3.5.1 Losses

During training, we define the loss functions for the semantic branch ℓ_{sem} , geometric branch ℓ_{geo} , and semantic-geometric feature grid fusion ℓ_{fus} as follows:

$$\begin{cases} \ell_{sem} = \ell_{ce}(\mathbf{s}, \bar{\mathbf{s}}) + \ell_{occ}(\mathbf{S}, \bar{\mathbf{S}}) \\ \ell_{geo} = \ell_{ce}(\mathbf{G}, \bar{\mathbf{G}}) \\ \ell_{fus} = \ell_{occ}(\mathbf{Y}, \bar{\mathbf{Y}}) + \ell_{ce}(\mathbf{y}, \bar{\mathbf{s}}) \end{cases} \quad (6)$$

where ℓ_{ce} denotes the weighted cross-entropy loss, with weights computed from class frequencies. ℓ_{occ} is a comprehensive occupancy loss, following prior work [4, 37, 38]. $\bar{\mathbf{G}}$ represents the ground-truth of geometry. We apply $\ell_{occ}(\mathbf{S}, \bar{\mathbf{S}})$ only to voxels containing more than one point, supervising voxel-level semantic learning.

3.5.2 Training Strategy

The training strategy of OccLE is summarized in Algorithm 1. In Phases I and II, we independently train the semantic and geometric branches. In Phase III, all modules are jointly optimized while freezing the geometric branch to prevent its overfitting.

Algorithm 1: The training strategy of OccLE

Input: Annotated dataset \mathcal{D}_l , unannotated dataset \mathcal{D}_u , Semantic branch Θ_{sem} , Geometric branch Θ_{geo} , Semantic-geometric feature grid fusion module Θ_{fus}

Output: Trained $\Theta_{sem}, \Theta_{geo}, \Theta_{fus}$

Phase I: Train the semantic branch

Train Θ_{sem} with dataset $\mathcal{D}_l, \mathcal{D}_u$, loss ℓ_{sem} , label $\{\bar{\mathbf{S}}, \bar{\mathbf{s}}\}$

Phase II: Train the geometric branch

Train the teacher model Θ_{geo-T} with dataset \mathcal{D}_l , loss ℓ_{sem} , label $\{\bar{\mathbf{G}}\}$

Predict $\{\bar{\mathbf{G}}_T\}$ for dataset \mathcal{D}_u via Θ_{geo-T}

Train the student model Θ_{geo-S} with dataset $\mathcal{D}_l, \mathcal{D}_u$, loss ℓ_{sem} , label $\{\bar{\mathbf{G}}\}, \{\bar{\mathbf{G}}_T\}$

Phase III: Train the semantic-geometric feature grid fusion module

Freeze Θ_{geo-S} ; Train Θ_{fus} and Θ_{sem} with dataset $\mathcal{D}_l, \mathcal{D}_u$, loss ℓ_{fus}, ℓ_{sem} , label $\{\bar{\mathbf{Y}}, \bar{\mathbf{s}}\}$

4 Experiment

4.1 Dataset and Metric

4.1.1 Dataset

We evaluate OccLE on the SemanticKITTI [27], which includes 22 outdoor driving scenarios: 10 sequences for training, 1 for validation, and 11 for testing. The dataset annotates scenes of size $51.2m \times 51.2m \times 6.4m$ with a voxel size of $0.2m \times 0.2m \times 0.2m$ for 20 semantic classes (19 semantics + 1 free). To simulate a label-efficient learning, we use only 10% of the voxel annotations from the training set, obtained via interval sampling.

4.1.2 Metric

There are two domain metrics: intersection over union (IoU) and mean intersection over union (mIoU) across 19 classes. IoU measures the overall scene completion quality, while mIoU evaluates the quality of semantic segmentation for each class. We use IoU as the primary metric for the geometric branch and mIoU as the primary metric for the semantic branch and semantic-geometric feature grid fusion.

4.2 Implementation Details

All experiments are conducted on 2 NVIDIA A6000 GPUs with a batch size of 1. The AdamW optimizer is used with an initial learning rate of $2e^{-4}$ and a weight decay of e^{-4} . The training duration is set to 40 epochs, except for the

teacher model in the geometric branch, which is set to 100 epochs. In the semantic branch, camera images are cropped into 1220×370 , and the downsampling scale of \mathcal{G}_{s2d} and \mathcal{G}_{s3d} is $8\times$; In the geometric branch, we utilize ResNet50 [39] and a 2-layer sparse Conv3D to extract features from image and LiDAR scans. In the semantic-geometric feature grid fusion module, we stack 4 Dual Mamba blocks.

4.3 Main Result

We present a quantitative comparison on the SemanticKITTI validation set in Table 2. OccLE obtains competitive performance, achieving 16.59 % mIoU and 39.96 % IoU. It surpasses all fully supervised camera-based methods (HASSC [40] with 40.66 % mIoU) and approaches the performance of fully supervised multi-modal methods (OccLoff [22] with 22.62 % mIoU). As illustrated in Figure 4, OccLE achieves strong performance in complex scenes, accurately reconstructing buildings and vegetation, and distinguishing small objects such as traffic signs and poles.

Table 2: Quantitative results on SemanticKITTI validation set. **Bold** and underline represent the best and second best results, respectively.

Method	Inp.	Sup.	IoU	mIoU	car (3.92%)	bicycle (0.03%)	motorcycle (0.03%)	truck (0.16%)	other-veh. (0.20%)	person (0.07%)	bicyclist (0.07%)	motorcyclist (0.05%)	road (15.30%)	parking (1.12%)	sidewalk (1.13%)	other-grnd.(0.56%)	building (14.10%)	fence (3.90%)	vegetation (39.3%)	trunk (0.51%)	terrain (9.17%)	pole (0.29%)	traf.-sign (0.08%)
TPVFormer [19]	C	Full	35.61	11.36	23.81	0.36	0.05	8.08	4.35	0.51	0.89	0.00	56.50	20.60	25.87	0.85	13.88	5.94	16.92	2.26	30.38	3.14	1.52
OccFormer [14]	C	Full	36.50	13.46	25.09	0.81	1.19	25.53	8.52	2.78	2.82	0.00	58.85	19.61	26.88	0.31	14.40	5.61	19.63	3.93	32.62	4.26	2.86
VoxFormer [4]	C	Full	44.15	13.35	25.64	1.28	0.56	7.26	7.81	1.93	1.97	0.00	53.57	19.69	26.52	0.42	19.54	7.31	26.10	6.10	33.06	9.15	4.94
PanoSSC [41]	C	Full	34.94	11.22	19.63	0.63	0.36	14.79	6.22	0.87	0.00	0.00	56.36	17.76	26.40	<u>0.88</u>	14.26	5.72	16.69	1.83	28.05	1.94	0.70
H2GFormer [32]	C	Full	44.69	14.29	28.21	0.95	0.91	6.80	9.32	1.15	0.10	0.00	57.00	<u>21.74</u>	29.37	0.34	20.51	7.98	27.44	7.80	36.26	9.88	5.81
OctreeOcc [42]	C	Full	44.71	13.12	28.07	0.64	0.71	16.43	6.03	2.25	2.57	0.00	55.13	18.68	26.74	0.65	18.69	4.01	25.26	4.89	32.47	3.72	2.36
SGN [38]	C	Full	<u>46.21</u>	15.32	33.31	0.61	0.46	6.03	9.84	0.47	0.10	0.00	59.10	19.05	29.41	0.33	25.17	9.96	28.93	9.58	38.12	13.25	7.32
Symphonies [37]	C	Full	41.44	13.44	27.23	1.44	2.28	15.99	9.52	3.19	8.09	0.00	55.78	14.57	26.77	0.19	18.76	6.18	24.50	4.32	28.49	8.99	5.39
HASSC [40]	C	Full	44.55	15.88	30.64	1.20	0.91	<u>23.72</u>	7.77	1.79	2.47	0.00	62.75	20.20	32.40	0.51	22.90	8.67	26.47	7.14	38.10	9.00	5.23
RenderOcc [6]	C	Full	-	12.87	24.90	0.37	0.28	6.03	3.66	1.91	3.11	0.00	57.2	16.11	28.44	0.91	18.18	9.10	26.23	4.87	33.61	6.24	3.38
OccLoff [22]	C+L	Full	-	22.62	<u>46.44</u>	2.08	3.91	20.38	8.72	3.88	4.35	0.00	66.25	21.07	43.51	0.57	41.23	15.86	41.20	20.06	46.21	27.60	16.47
OccFusion [5]	C+L	Full	58.68	<u>21.92</u>	<u>45.62</u>	2.96	3.51	20.05	8.76	3.16	<u>4.37</u>	0.00	<u>65.67</u>	23.08	<u>36.33</u>	0.00	<u>39.09</u>	<u>15.70</u>	45.53	<u>19.37</u>	<u>45.53</u>	<u>27.57</u>	<u>15.21</u>
OccGen [23]	C+L	Full	36.87	13.74	26.83	1.60	2.53	15.49	12.83	<u>3.20</u>	3.37	0.00	61.28	20.42	28.30	0.43	14.49	6.94	20.04	3.94	32.44	4.11	2.77
RenderOcc [6]	C	Self	-	8.24	14.83	0.42	0.17	2.47	1.78	0.94	3.20	0.00	43.64	12.54	19.10	0.00	11.59	4.71	17.61	1.48	20.01	1.17	0.88
OccLE(Ours)	C+L	10%	40.60	16.59	37.27	<u>2.76</u>	4.39	0.90	<u>10.88</u>	2.52	0.09	0.00	55.79	19.96	28.85	0.14	24.56	12.53	35.19	16.98	35.29	17.16	10.01

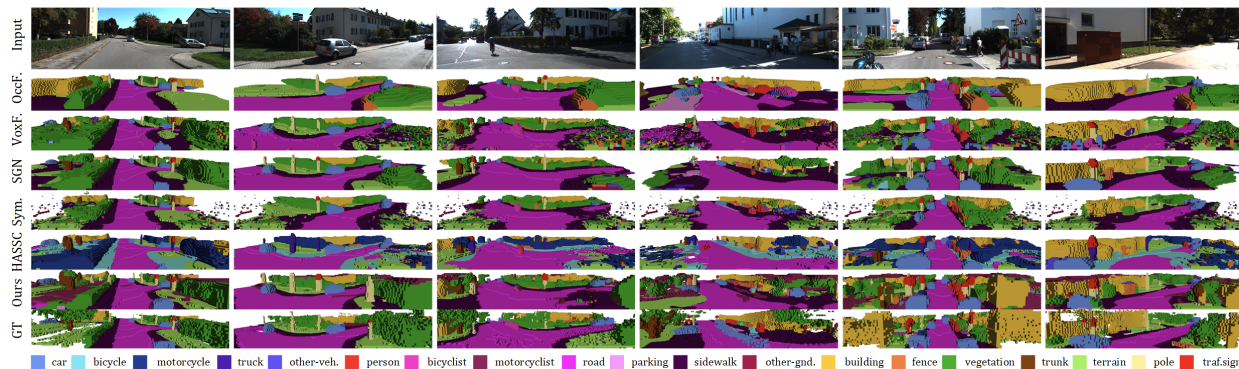


Figure 4: Qualitative results on the SemanticKITTI validation set. OccF., VoxF., SGN, Sym., and HASSC represent the prediction results from [14], [4], [38], [37], and [40], respectively. GT denotes the ground truth.

4.4 Ablation Studies

We conduct all ablation studies on the validation set of the SemanticKITTI dataset. We focus on three aspects: semantic branch, geometric branch, and overall pipeline.

4.4.1 The Semantic Branch

To evaluate the extractor and pseudo label in the semantic branch, for comparison, we adopt ESPNetv2 [43] and MobileNet [44] as \mathcal{G}_{s2d} , employ 1-layer and 2-layer versions of sparse UNet3D as \mathcal{G}_{s3d} , and train using unaligned pseudo labels. As depicted in Table 3, 2D extractors designed for edge device suffer a notable performance degradation, whereas our method achieves the highest mIoU(s) while retaining remaining lightweight. Increasing the depth of the sparse UNet3D architecture improves mIoU(S) without substantially increasing computational cost. Moreover, aligned pseudo labels yield a significant mIoU gain by providing supervision for unaligned classes.

Table 3: Ablation study of the semantic branch. The unit of Inf. Time is in milliseconds.

\mathcal{G}_{s2d}	Inf. Time	mIoU(s)	\mathcal{G}_{s3d}	Inf. Time	mIoU(S)
ESPNetv2	4.38	28.71	1-layer	41.77	12.38
MobileNet	6.10	48.76	2-layer	43.22	13.30
Ours (w/o align.)	6.87	41.89	Ours (w/o align.)	44.59	9.89
Ours (w/ align.)	6.87	51.51	Ours (w/ align.)	44.59	13.94

4.4.2 The Geometric Branch

To evaluate the effects of model architecture and training strategy in the geometric branch, we design a baseline that employs Conv3D and 3D DA for feature extraction and interaction, and compare our semi-supervision against full supervision. As depicted in Table 4(a), our cross-plane image and LiDAR feature synergy only has a minor precision drop while significantly reducing module inference time from 138.62 ms to 26.08 ms. Our data augmentation strategy boosts student model performance as augmentation degree increases. Under semi-supervision, our student model reaches 53.60 IoU, closely approaching the fully supervised performance of 56.77 IoU.

Table 4: Ablation studies for (a) geometric branch and (b) overall pipeline. “weak,” “medium,” and “strong” denote the degrees of data augmentation, -S and -T represents the student and teacher models. ‘Sem.’, ‘Geo.’, and ‘Proj.’ denote the semantic branch, geometric branch, and supervising with scatter-accumulated projection, respectively.

(a) Geometric branch.						(b) Overall pipeline.						
Sup.	Weak	Middle	Strong	Model	IoU	Sup.	Sem.	Geo.	Proj.	Model	mIoU	IoU
Full				Ours-T	56.77	Full	✓	✓	✓	Ours	20.32	51.73
10%	✓			Baseline	52.79	10%				Baseline	9.64	22.30
10%	✓			Ours-T	52.66	10%	✓		✓	Ours	11.84	27.46
10%	✓			Ours-S	52.86	10%		✓	✓	Ours	8.08	17.52
10%	✓	✓		Ours-S	52.88	10%	✓	✓		Ours	11.55	18.52
10%	✓	✓	✓	Ours-S	53.60	10%	✓	✓	✓	Ours	16.59	40.60

4.4.3 Overall Pipeline

As depicted in Table 4(b), compared to the baseline, our method increases mIoU from 9.64 to 16.59 using only 10% voxel annotations, closely approaching the fully supervised performance of 20.32 mIoU. Furthermore, ablating any module in OccLE results in a precision drop, demonstrating the essential role of these three modules in label-efficient learning. Additional ablation studies are presented in the Appendix C.2.

5 Conclusion

In this paper, we propose OccLE, a label-efficient 3D semantic occupancy prediction that leverages limited voxel annotations while preserving high performance. OccLE incorporates three key components: (1) distilling 2D foundation model to predict aligned pseudo label for supervising 2D and 3D semantic learning, (2) cross-plane image and LiDAR feature synergy for efficient geometry learning under semi-supervision, and (3) semantic-geometric feature grid fusion with Dual Mamba and scatter-accumulated projection for supervising unannotated regions. Experimental results demonstrate that OccLE achieves an mIoU of 16.59% on the SemanticKITTI validation set using only 10% of the voxel annotations.

References

- [1] S. Song, F. Yu, A. Zeng, A. X. Chang, M. Savva, and T. Funkhouser, “Semantic scene completion from a single depth image,” in *IEEE Conf. Comput. Vis. Pattern Recog.*, 2017, pp. 1746–1754.
- [2] Y.-J. Li, J. Park, M. O’Toole, and K. Kitani, “Modality-agnostic learning for radar-lidar fusion in vehicle detection,” in *IEEE Conf. Comput. Vis. Pattern Recog.*, 2022, pp. 918–927.
- [3] N. Fang, L. Qiu, S. Zhang, Z. Wang, K. Hu, and K. Wang, “A cross-scale hierarchical transformer with correspondence-augmented attention for inferring bird’s-eye-view semantic segmentation,” *IEEE Trans. Intell. Transp. Syst.*, 2024.
- [4] Y. Li, Z. Yu, C. Choy, C. Xiao, J. M. Alvarez, S. Fidler, C. Feng, and A. Anandkumar, “Voxformer: Sparse voxel transformer for camera-based 3d semantic scene completion,” in *IEEE Conf. Comput. Vis. Pattern Recog.*, 2023, pp. 9087–9098.
- [5] Z. Ming, J. S. Berrio, M. Shan, and S. Worrall, “Occfusion: Multi-sensor fusion framework for 3d semantic occupancy prediction,” *IEEE Trans. Intell. Veh.*, 2024.
- [6] M. Pan, J. Liu, R. Zhang, P. Huang, X. Li, H. Xie, B. Wang, L. Liu, and S. Zhang, “Renderocc: Vision-centric 3d occupancy prediction with 2d rendering supervision,” in *IEEE Int. Conf. Robot. Autom.*, 2024, pp. 12 404–12 411.
- [7] Y. Huang, W. Zheng, B. Zhang, J. Zhou, and J. Lu, “Selfocc: Self-supervised vision-based 3d occupancy prediction,” in *IEEE Conf. Comput. Vis. Pattern Recog.*, 2024, pp. 19 946–19 956.
- [8] N. Ravi, V. Gabeur, Y.-T. Hu, R. Hu, C. Ryali, T. Ma, H. Khedr, R. Rädle, C. Rolland, L. Gustafson *et al.*, “Sam 2: Segment anything in images and videos,” *arXiv preprint arXiv:2408.00714*, 2024.
- [9] W. Yin, C. Zhang, H. Chen, Z. Cai, G. Yu, K. Wang, X. Chen, and C. Shen, “Metric3d: Towards zero-shot metric 3d prediction from a single image,” in *IEEE Conf. Comput. Vis. Pattern Recog.*, 2023, pp. 9043–9053.
- [10] X. Zhu, H. Zhou, T. Wang, F. Hong, Y. Ma, W. Li, H. Li, and D. Lin, “Cylindrical and asymmetrical 3d convolution networks for lidar segmentation,” in *IEEE Conf. Comput. Vis. Pattern Recog.*, 2021, pp. 9939–9948.
- [11] H. Jiang, L. Liu, T. Cheng, X. Wang, T. Lin, Z. Su, W. Liu, and X. Wang, “Gausstr: Foundation model-aligned gaussian transformer for self-supervised 3d spatial understanding,” *arXiv preprint arXiv:2412.13193*, 2024.
- [12] S. Boeder, F. Gigengack, and B. Risse, “Occflownet: Towards self-supervised occupancy estimation via differentiable rendering and occupancy flow,” *arXiv preprint arXiv:2402.12792*, 2024.
- [13] A.-Q. Cao and R. De Charette, “Monoscene: Monocular 3d semantic scene completion,” in *IEEE Conf. Comput. Vis. Pattern Recog.*, 2022, pp. 3991–4001.
- [14] Y. Zhang, Z. Zhu, and D. Du, “Occformer: Dual-path transformer for vision-based 3d semantic occupancy prediction,” in *Int. Conf. Comput. Vis.*, 2023, pp. 9433–9443.
- [15] Y. Wei, L. Zhao, W. Zheng, Z. Zhu, J. Zhou, and J. Lu, “Surroundocc: Multi-camera 3d occupancy prediction for autonomous driving,” in *Int. Conf. Comput. Vis.*, 2023, pp. 21 729–21 740.
- [16] J. Li, X. He, C. Zhou, X. Cheng, Y. Wen, and D. Zhang, “Viewformer: Exploring spatiotemporal modeling for multi-view 3d occupancy perception via view-guided transformers,” in *Eur. Conf. Comput. Vis.*, 2025, pp. 90–106.
- [17] A. Gu and T. Dao, “Mamba: Linear-time sequence modeling with selective state spaces,” *arXiv preprint arXiv:2312.00752*, 2023.
- [18] Y. Huang, W. Zheng, Y. Zhang, J. Zhou, and J. Lu, “Gaussianformer: Scene as gaussians for vision-based 3d semantic occupancy prediction,” in *Eur. Conf. Comput. Vis.*, 2025, pp. 376–393.
- [19] ———, “Tri-perspective view for vision-based 3d semantic occupancy prediction,” in *IEEE Conf. Comput. Vis. Pattern Recog.*, 2023, pp. 9223–9232.
- [20] L. Yang, L. Zheng, W. Ai, M. Liu, S. Li, Q. Lin, S. Yan, J. Bai, Z. Ma, and X. Zhu, “Metaocc: Surround-view 4d radar and camera fusion framework for 3d occupancy prediction with dual training strategies,” *arXiv preprint arXiv:2501.15384*, 2025.
- [21] J. Zhang, Y. Ding, and Z. Liu, “Occfusion: Depth estimation free multi-sensor fusion for 3d occupancy prediction,” in *Proc. Asian Conf. Comput. Vis.*, 2024, pp. 3587–3604.
- [22] ———, “Occloff: Learning optimized feature fusion for 3d occupancy prediction,” in *IEEE/CVF Winter Conf. Appl. Comput. Vis.*, pp. 3096–3106.
- [23] G. Wang, Z. Wang, P. Tang, J. Zheng, X. Ren, B. Feng, and C. Ma, “Occgen: Generative multi-modal 3d occupancy prediction for autonomous driving,” in *Eur. Conf. Comput. Vis.*, 2025, pp. 95–112.
- [24] D. Berthelot, N. Carlini, I. Goodfellow, N. Papernot, A. Oliver, and C. A. Raffel, “Mixmatch: A holistic approach to semi-supervised learning,” *Adv. Neural Inf. Process. Syst.*, vol. 32, 2019.
- [25] J. Gui, T. Chen, J. Zhang, Q. Cao, Z. Sun, H. Luo, and D. Tao, “A survey on self-supervised learning: Algorithms, applications, and future trends,” *IEEE Trans. Pattern Anal. Mach. Intell.*, 2024.
- [26] M. Cordts, M. Omran, S. Ramos, T. Rehfeld, M. Enzweiler, R. Benenson, U. Franke, S. Roth, and B. Schiele, “The cityscapes dataset for semantic urban scene understanding,” in *IEEE Conf. Comput. Vis. Pattern Recog.*, 2016, pp. 3213–3223.

- [27] J. Behley, M. Garbade, A. Milioto, J. Quenzel, S. Behnke, C. Stachniss, and J. Gall, “Semantickitti: A dataset for semantic scene understanding of lidar sequences,” in *Int. Conf. Comput. Vis.*, 2019, pp. 9297–9307.
- [28] J. Lambert, Z. Liu, O. Sener, J. Hays, and V. Koltun, “Mseg: A composite dataset for multi-domain semantic segmentation,” in *IEEE Conf. Comput. Vis. Pattern Recog.*, 2020, pp. 2879–2888.
- [29] O. Ronneberger, P. Fischer, and T. Brox, “U-net: Convolutional networks for biomedical image segmentation,” in *Int. Conf. Med. Image Comput. & Comput.-Assist. Intervent.*, 2015, pp. 234–241.
- [30] Y. Zhou and O. Tuzel, “Voxelnet: End-to-end learning for point cloud based 3d object detection,” in *IEEE Conf. Comput. Vis. Pattern Recog.*, 2018, pp. 4490–4499.
- [31] Y. Yan, Y. Mao, and B. Li, “Second: Sparsely embedded convolutional detection,” *Sensors*, 2018.
- [32] Y. Wang and C. Tong, “H2gformer: Horizontal-to-global voxel transformer for 3d semantic scene completion,” in *AAAI*, vol. 38, no. 6, 2024, pp. 5722–5730.
- [33] J. Zhang, Y. Zhang, Q. Liu, and Y. Wang, “Lightweight spatial embedding for vision-based 3d occupancy prediction,” *arXiv preprint arXiv:2412.05976*, 2024.
- [34] Y. Xue, R. Li, F. Wu, Z. Tang, K. Li, and M. Duan, “Bi-ssc: Geometric-semantic bidirectional fusion for camera-based 3d semantic scene completion,” in *IEEE Conf. Comput. Vis. Pattern Recog.*, 2024, pp. 20 124–20 134.
- [35] L. Yang, L. Qi, L. Feng, W. Zhang, and Y. Shi, “Revisiting weak-to-strong consistency in semi-supervised semantic segmentation,” in *IEEE Conf. Comput. Vis. Pattern Recog.*, 2023, pp. 7236–7246.
- [36] H. Li, Y. Hou, X. Xing, Y. Ma, X. Sun, and Y. Zhang, “Occmamba: Semantic occupancy prediction with state space models,” *arXiv preprint arXiv:2408.09859*, 2024.
- [37] H. Jiang, T. Cheng, N. Gao, H. Zhang, T. Lin, W. Liu, and X. Wang, “Symphonize 3d semantic scene completion with contextual instance queries,” in *IEEE Conf. Comput. Vis. Pattern Recog.*, 2024, pp. 20 258–20 267.
- [38] J. Mei, Y. Yang, M. Wang, J. Zhu, J. Ra, Y. Ma, L. Li, and Y. Liu, “Camera-based 3d semantic scene completion with sparse guidance network,” *IEEE Trans. Image Process.*, 2024.
- [39] K. He, X. Zhang, S. Ren, and J. Sun, “Deep residual learning for image recognition,” in *IEEE Conf. Comput. Vis. Pattern Recog.*, 2016, pp. 770–778.
- [40] S. Wang, J. Yu, W. Li, W. Liu, X. Liu, J. Chen, and J. Zhu, “Not all voxels are equal: Hardness-aware semantic scene completion with self-distillation,” in *IEEE Conf. Comput. Vis. Pattern Recog.*, 2024, pp. 14 792–14 801.
- [41] Y. Shi, J. Li, K. Jiang, K. Wang, Y. Wang, M. Yang, and D. Yang, “Panossc: Exploring monocular panoptic 3d scene reconstruction for autonomous driving,” in *Int. Conf. 3D Vision*, 2024, pp. 1219–1228.
- [42] Y. Lu, X. Zhu, T. Wang, and Y. Ma, “Octreeocc: Efficient and multi-granularity occupancy prediction using octree queries,” *arXiv preprint arXiv:2312.03774*, 2023.
- [43] S. Mehta, M. Rastegari, L. Shapiro, and H. Hajishirzi, “Espnetv2: A light-weight, power efficient, and general purpose convolutional neural network,” in *IEEE Conf. Comput. Vis. Pattern Recog.*, 2019, pp. 9190–9200.
- [44] A. G. Howard, “Mobilenets: Efficient convolutional neural networks for mobile vision applications,” *arXiv preprint arXiv:1704.04861*, 2017.
- [45] D. Hilbert, *Dritter Band: Analysis· Grundlagen der Mathematik· Physik Verschiedenes: Nebst Einer Lebensgeschichte*. Springer-Verlag, 2013.

A Dual Mamba Structure

The detailed structure of Dual Mamba is illustrated in Fig. A1. The model employs a U-Net backbone with four downsampling stages and four upsampling stages. Each stage incorporates a dual Mamba block. Within a dual Mamba block, two parallel branches compute positional embeddings for the two inputs and then exchange their feature channels prior to reordering. We use a Hilbert curve [45] to linearize the 3D representation into a 1D sequence, apply a Mamba block to capture long-range dependencies, and finally restore the three-dimensional structure.

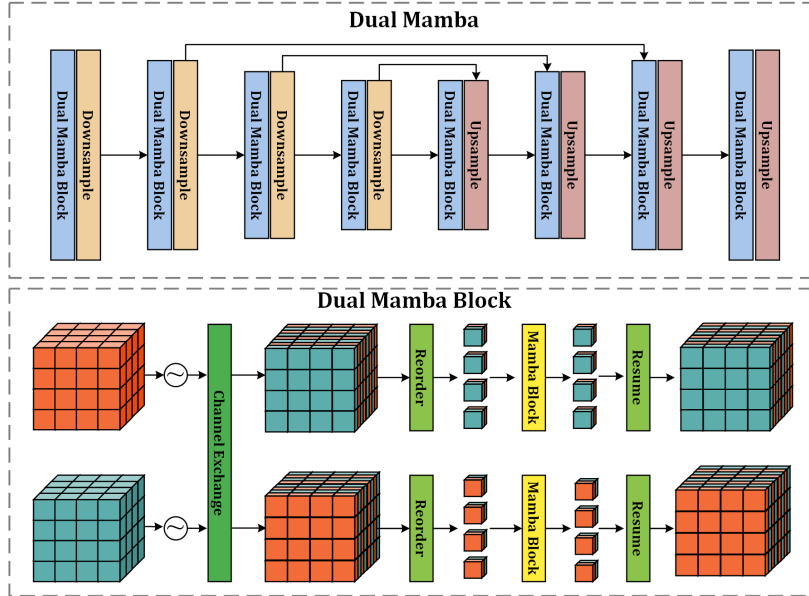


Figure A1: The detailed structure of Dual Mamba. It comprises four stages and employs two parallel branches to process the inputs at each stage.

B Aligned Label Generation

We employ dataset-specific and open-vocabulary segmentation 2D foundation models to generate aligned pseudo labels. The class mappings are listed in Table B.1. We utilize SAM2 [8] to produce trunk class labels and integrate them into the MSeg [28] outputs. This example illustrates our aligned pseudo label generation process, which can scale to any dataset with different class taxonomies.

C Supplementary Experimental Results

C.1 Supplementary Ablation Study

We evaluate some experimental setting in Table C.2. To assess the impact of semi-supervision in the geometric branch on the overall pipeline, we incorporated a teacher model of the geometric branch into final joint training. The results indicate that mIoU and IoU decrease by 0.42 and 1.74, respectively.

We compare our scatter-accumulated projection method with an alternative approach that weights features by the distance between each voxel and the camera. The latter method yields a 3.21 mIoU drop. This result demonstrates that the scatter-accumulated projection is simple yet effective in supervising all voxels with aligned pseudo labels, whereas the distance-weighted projection reduces supervision quality for distant voxels.

We assess the necessity of using limited voxel annotations rather than relying solely on aligned pseudo labels. Our experiments indicate that relying solely on aligned pseudo labels results in a marked decline in precision, signaling pattern collapse during training when voxel annotations are absent. These results confirm that voxel annotations are essential for guiding the model toward an effective fusion of semantic and geometric features.

Table B.1: The aligned label generation.

SemantiKITTI		Image Segmentation		SemantiKITTI		Image Segmentation	
Label	Class	Label	Class	Label	Class	Label	Class
0	free			12	other-grnd.	31	road_barrier
1	car	176	car			32	mailbox
2	bicycle	175	bicycle			137	fire_hydrant
3	motorcycle	178	motorcycle			191	wall
				13	building	35	building
4	truck	182	truck	14	fence	144	fence
5	other.-veh.	177	autorickshaw	15	vegetation	131	road_barrier
		180	bus			174	vegetation
		181	train	16	trunk	SAM2	trunk
		183	trailer	17	terrain	102	terrain
		185	slow_wheeled_object	18	pole	143	pole
6	person	125	person			130	streetlight
7	bicyclist	126	rider_other			145	railing_banister
		127	bicyclist			146	guard_rail
8	motorcyclist	128	motorcyclist			162	column
9	road	98	road	19	traf.-sign.	135	traffic_sign
10	parking	138	parking_meter			136	traffic_light
11	sidewalk	100	sidewalk_pavement				

Table C.2: Supplementary ablation study.

Model	mIoU	IoU
w/ geometric teacher model	16.17	38.86
w/ weighted projection	13.38	40.40
w/o limited voxel annotation	0.37	7.84
Ours	16.59	40.60

C.2 Supplementary Qualitative Comparison

We show additional qualitative results of OccLE on the SemanticKITTI validation dataset in Figure C1. OccLE maintains strong performance across varied scenes, delivering effective scene completion and precise class classification.

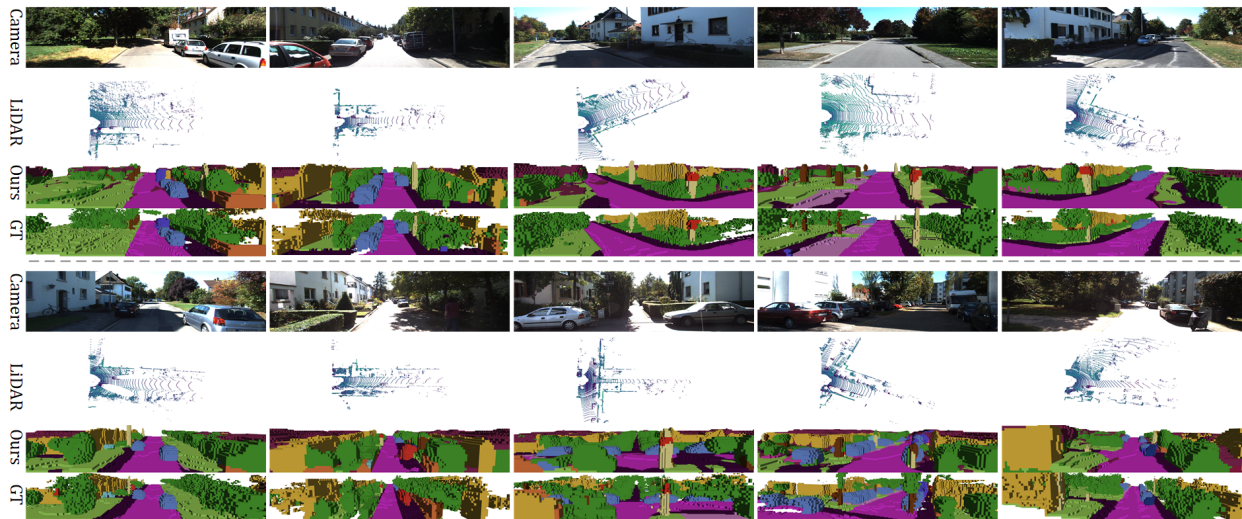


Figure C1: The qualitative results of OccLE on SemanticKITTI validation dataset.

D Limitation

In this study, we simulate label-efficient learning for 3D semantic occupancy prediction by uniformly sampling 10% of voxel annotations across all scenes in the SemanticKITTI dataset. This strategy ensures the generalization across diverse scenes. However, concentrating limited voxel annotations within a few scenes may lead to overfitting, thereby diminishing the robustness of OccLE in unfamiliar scenes. Consequently, for real-world autonomous driving applications, it is advisable to distribute limited voxel annotations across a wide range of scenes, enhancing its performance in varied and unseen environments.